A broadband low-reflection metamaterial absorber

S. Gu,[a] J. P. Barrett, T. H. Hand, B.-I. Popa, and S. A. Cummer[a]
Department of Electrical and Computer Engineering and Center for Metamaterials and Integrated Plasmonics, Duke University, Durham, North Carolina 27705, USA

(Received 2 February 2010; accepted 2 August 2010; published online 30 September 2010)

Artificially engineered metamaterials have enabled the creation of electromagnetic materials with properties not found in nature. Recent work has demonstrated the feasibility of developing high performance, narrowband electromagnetic absorbers using such metamaterials. These metamaterials derive their absorption properties primarily through dielectric loss and impedance matching at resonance. This paper builds on that work by increasing the bandwidth through embedding resistors into the metamaterial structure in order to lower the Q factor and by using multiple elements with different resonances. This is done while maintaining an impedance-matched material at normal incidence. We thus present the design, simulation, and experimental verification of a broadband gigahertz region metamaterial absorber, with a maximum absorption of 99.9% at 2.4 GHz, and a full width at half maximum bandwidth of 700 MHz, all while maintaining low reflection inside and outside of resonance. © *2010 American Institute of Physics*. [doi:10.1063/1.3485808]

I. INTRODUCTION

The properties of materials with electromagnetic properties not found in nature were theorized by Veselago,[1] who showed many of the unusual properties of materials with simultaneously negative permittivity, ϵ, and permeability, μ. Recent research in metamaterials have led to practical implementations of such materials. One of the earliest approaches for realizing complex electromagnetic metamaterials utilizes split ring resonators (SRRs) to generate a Lorentzian-shaped resonant magnetic response, along with thin wires to generate a broadband electrical response.[2] Alternating layers of these electrically small SRRs and thin wires, with largest dimension $\ll\lambda$, will produce a simultaneously negative ϵ_r and μ_r.[3] Subsequent experiments using a two-dimensional array of copper strips and SRRs experimentally verified the negative refraction properties of such metamaterials.[4] Another method of generating an electrical response is with an electrically coupled LC resonator (ELC).[5] Unlike thin wires, ELCs are resonant structures that exhibit a Lorentzian response similar to that of the SRR, except in permittivity instead of in permeability. Alternating layers of tuned SRRs and ELCs have been shown to result in simultaneously negative ϵ_r and μ_r, resulting in negative refraction.[6]

Prior to the introduction of metamaterials, most of the work on rf absorbers was focused on rf absorbing materials commonly found as carbon loaded foam pyramidal absorbers, ferrite tiles, and engineered frequency selective surfaces (FSS). Pyramidal absorbers are relatively effective, and are broadband, but are typically bulky because they need to be on the order of $\lambda/2$ or greater to achieve significant attenuation. A FSS derives its bandfiltering absorption/reflection properties from its periodic spacing, and is typically implemented using periodically perforated metallic screens or as metallic particles on a dielectric substrate.[7] Recent advances in FSS include the use of genetic algorithms and Pareto optimizations to synthesize broadband, multilayer FSS.[8] These FSS have been used in designs for a considerable time and have been quite successful. However, due to their periodic structure and structures comparable to wavelength, challenges remain with unwanted passbands, off-normal incidence, and polarizations. These challenges have led to the development of alternative materials and structures that exhibit bulk absorption, including metamaterial absorbers that are the focus of this paper.

Metamaterial absorbers utilizing variations in three basic structures, SRRs, ELCs, and thin wires, can be used to absorb electromagnetic energy through resistive and/or dielectric loss. Landy, *et al.*[9] demonstrated a near perfect narrow band absorber in the THz region by using an electric-SRR, copper strip, and dielectric based metamaterial. It was shown that most of the loss was due to dielectric loss.[9] Subsequent work replaced the copper strip with a complete backplane, creating a 16 μm thick narrow band absorber with 96% maximum absorption at 1.6 THz that had good off-normal incidence performance for both TE and TM modes.[10]

II. DESIGN

In this paper, we present the design, simulation, and experimental testing of a gigahertz region metamaterial absorber that uses a combination of ELCs and SRRs to achieve 99% absorption at 2.4 GHz with a full width at half maximum (FWHM) of 700 MHz. The design of this absorber differs from previous work in its use of lumped resistive elements as the chief contributor of absorption. Furthermore, this absorber is designed to be a normal-incidence impedance matched material (i.e., $z=1$), both in and out of resonance, and therefore does not have a reflective backplane. This differs from the metamaterial designs used in Landy, *et al.* and Tao, *et al.* which were perfectly matched at resonance but had high reflection out of band. Thus, this metamaterial design is an absorber/transmitter rather than an absorber/reflector. The use of resistors and a backplane-less metama-

[a]Electronic addresses: sg58@duke.edu and cummer@ee.duke.edu.

terial design was mentioned by Bilotti,[11] but was not experimentally tested and did not utilize the concept of using impedance matching to decrease reflection.

The theoretical basis for this design comes from the relationships between the effective relative permittivity, relative permeability, index of refraction, and impedance (ϵ_r, μ_r, n, and z) of the SRR and ELC based media. As long as the SRR and ELC are electrically small, these bulk parameters hold and are related by the following equations:

$$z = \sqrt{\mu_r/\epsilon_r}, \tag{1}$$

$$n = \sqrt{\mu_r \epsilon_r}. \tag{2}$$

To create an absorber, we are interested in the values of n, ϵ_r, and μ_r where the incident electromagnetic field is attenuated inside the effective medium of the particle. For a right handed, passive material, using the $e^{+j\omega t}$ time convention, propagation loss corresponds primarily to $\mathrm{Im}(n)<0$. In Landy, *et al.*,[12] it is shown that for materials with complex μ and ϵ, the total loss depends on both $\mathrm{Im}(n)$ and $\mathrm{Im}(z)$. However, since our design aims for $z=1$ to reduce reflection, loss is dominated by $\mathrm{Im}(n)$.

Increasingly larger magnitudes of ϵ_r and μ_r will result in greater loss. The physical explanation is that a higher index material will have larger fields in the material, and thus more loss from dielectric and resistive heating. In addition, we would like to reduce reflection so that more power can be absorbed. This can be achieved by making $\epsilon_r=\mu_r$ so that $z=1$ for all frequencies.

In practice, loss is measured by the amount of electromagnetic power absorbed, where absorbed power, $A(\omega)$, is related to the reflected power, $R(\omega)$, the transmitted power, $T(\omega)$, and the reflection coefficient $S11$ and transmission coefficient $S21$ by $A(\omega)=1-R(\omega)-T(\omega)$ and $A(\omega)=1-|S11|^2-|S21|^2$, where $A(\omega)$, $R(\omega)$, and $T(\omega)$ are relative to the incident power. Furthermore, since the SRR and ELC particles are essentially *RLC* resonators,[2] one can change the resonant frequency $\omega_0=1/\sqrt{LC}$ and Q factor $Q=(1/R)\sqrt{L/C}$ by changing R, L, and C. Inductance and capacitance values, L and C, are adjusted in order to tune the strong, Lorentzian magnetic response of the SRR such that it overlays the strong Lorentzian electric response of the ELC to create a lossy, yet perfectly matched effective medium. Once this is accomplished, R can be adjusted to achieve the desired Q factor, whereby an increase in R yields a flatter, lower Q factor, and a decrease in R yields a sharper, higher Q factor.

Since the design of the absorber depends on optimizing the bulk parameters of ϵ_r and μ_r, an appropriate retrieval method is required. There exist several homogenization schemes that attach effective material parameters to media obtained from replicating elements such as those presented in Figs. 1(a) and 2. Thus, both theoretical[2,13–17] and numerical[18–21] approaches have been proposed that retrieve these effective parameters either directly, from the geometry of the particles, or indirectly by averaging the fields produced by them. For the purpose of our study, we need a retrieval method capable of characterizing the scattering off the absorbing media, as opposed to a method that describes in detail the physics of how individual cells behave. We therefore chose a relatively simple retrieval algorithm[19] that was shown to be successful in the design of various metamaterial devices,[22–24] and which implicitly accounts for complex phenomena such as spatial dispersion or coupling between constitutive elements. This method is especially suitable for experimental retrievals and relies on estimating the nonlocal effective refractive index and impedance from reflection and transmission measurements. Although this retrieval method does not necessarily describe correctly the internal physics of the unit-cell response, it is nevertheless an effective approach for describing the reflected and transmitted fields produced by the composite, which is our interest.

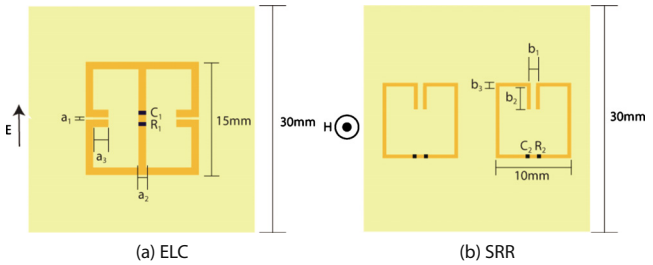

FIG. 1. (Color online) The optimum single-cell ELC-SRR absorption was achieved with (a) ELC parameters of $a_1=0.35$ mm, $a_2=1$ mm, $a_3=0$ mm, $C_1=10$ pF, and $R_1=10$ Ω, and (b) SRR parameters of $b_1=0.7$ mm, $b_2=3$ mm, $b_3=0.5$ mm, $C_2=10$ pF, and $R_2=5$ Ω.

One unit cell of an ELC and an SRR structure (composed of two identical SRRs for increased magnetic response) is depicted in Fig. 1. The FR4 dielectric was simulated with $\epsilon_r=4.4$ and is 0.2 mm thick. The copper traces are simulated to be 0.017 mm thick. The capacitive gaps, lumped capacitors, and lumped resistors were tuned such that the resonant frequencies of the ELC and SRRs were identical, and to optimize for bandwidth and peak absorption. Please note that for the initial ELC-SRR design, the width of the ELCs capacitive gap, a_3, was adjusted so that the resonant frequency of the ELC was similar to that of the SRR. The optimal solution was actually $a_3=0$ mm for that particular ELC-SRR arrangement, as noted in the caption. However, subsequent designs such as the ELC-SRR sandwich depicted in Fig. 6 were composed of various ELCs with $a_3>0$ mm in order to match resonance with the sandwiched SRRs.

By combining these two types of particles, an ELC-SRR was created and simulated using Ansoft HFSS, a commercial finite element solver of Maxwell's equations. Several arrangements were simulated, with the constraints that the ELC-SRR had to be much smaller than the wavelength, and

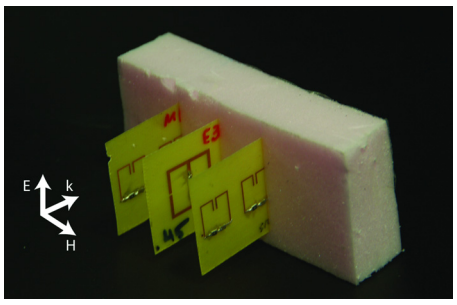

FIG. 2. (Color online) ELC-SRR.

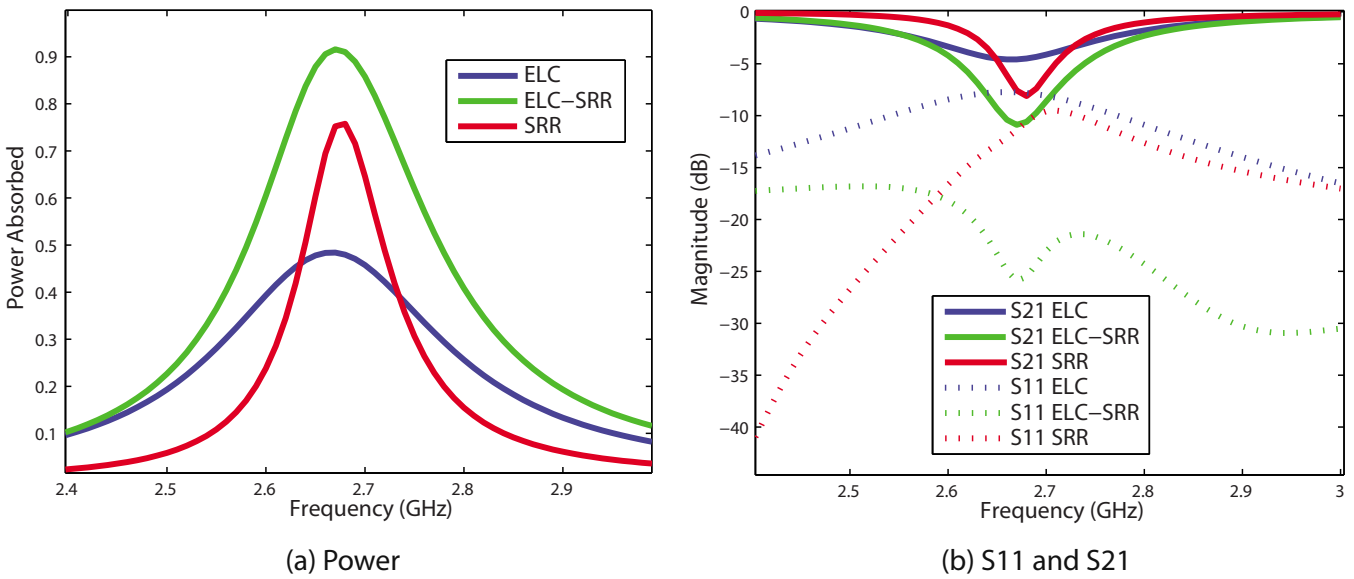

FIG. 3. (Color online) Simulated separate and combined ELC-SRR performance. (a) ELC-SRR absorption is higher and broader than individual ELC and SRR particles. (b) ELC-SRR achieves high absorption through decreased transmission (S21) and low reflection (S11).

that the ELCs and SRRs were arranged in such a way as to fit as many of them in per unit volume, to maximize absorption per unit volume, while reducing cross coupling between the constituent particles as much as possible.

The design that optimized these benchmarks is shown in Fig. 2. Its simulated response, along with that of just the ELC and SRR is shown in Fig. 3. 95% absorption was achieved at 2.65 GHz, with a FWHM of 300 MHz. Furthermore, the reflected power is below 5% throughout the range, indicating a well-matched effective medium. The parameter retrievals in Fig. 4 indicate that this high-absorption, low-reflection performance is due to the aforementioned similarity between the ϵ_r and μ_r responses. These simulations were thus consistent with theory, and provided a basis for experimental testing.

III. FABRICATION AND EXPERIMENT

The ELCs and SRRs were fabricated separately by using optical mask lithography to etch 0.017 mm thick copper traces on one side of a 0.2 mm thick FR4 dielectric. Once fabricated, the lumped resistors and capacitors were soldered

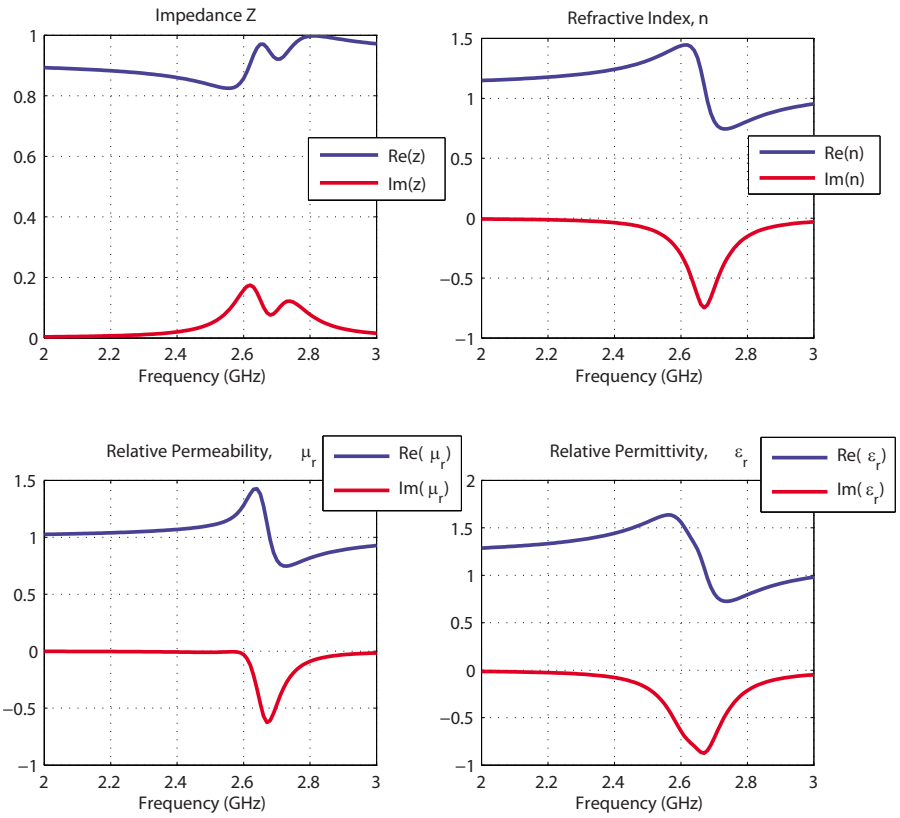

FIG. 4. (Color online) ELC-SRR retrievals. Permeability (μ_r) and permittivity (ϵ_r) have similar Lorentzian resonances around 2.67 GHz. Z is therefore near unity and Im(n) is large.

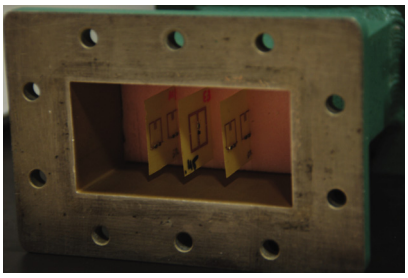

(a) ELC-SRR in WR340 Waveguide

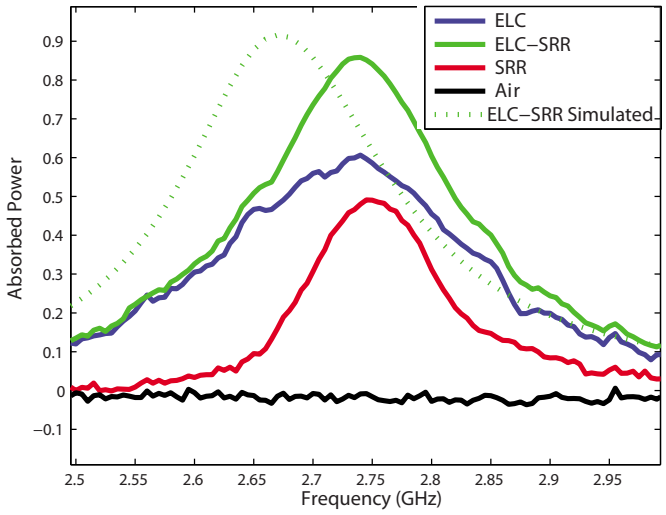

(b) Power

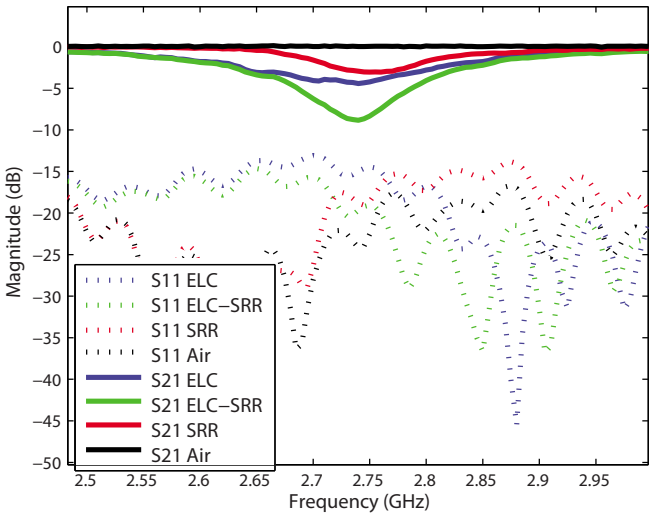

(c) S11 and S21

FIG. 5. (Color online) Experimental separate and combined ELC-SRR performance. (a) ELC-SRR measured in a WR340 closed waveguide. (b) ELC-SRR has the highest and broadest absorption with a 86% peak at 2.74 GHz, and FWHM bandwidth of 170 MHz. (c) ELC-SRR has deepest transmission (S21) dip and maintains comparatively low reflection (S11).

on. One unit cell of the absorber structure was mounted on a foam support and measurements were taken on a WR340 closed waveguide between 2–3 GHz, shown in Fig. 5(a). At these frequencies, propagation is confined to the TE_{10} mode. Reflection and transmission measurements, S11 and S21, were made for one unit cell of the ELC-SRR absorber as well as for just the constituent ELC and SRR particles. Figure 5(c) shows that the ELC-SRR has the deepest and broadest transmission minima, and moreover, has the lowest reflection. This result is strong evidence that the ELC-SRR is able to achieve greater absorption with minimal reflection at resonance by being simultaneously well matched and lossy. Note that S11 for air exhibits some reflection below −15 dB. This error is due to imperfect waveguide matching and is small enough to not affect experimental results. Figure 5(b) shows the calculated absorbed power, and the ELC-SRR is able to achieve 86% absorption at 2.74 GHz with a FWHM bandwidth of 170 MHz. These experimental results in Fig. 5 agree well with the simulated results in Fig. 3. Most importantly, the combined ELC-SRR has the highest and broadest absorption. One does note, however, that the ELC-SRR experimental peak of 2.74 GHz is shifted approximately 70 MHz higher compared to the simulated peak of 2.67 GHz in Fig. 5. This higher resonant frequency is likely due to the smaller experimental capacitances (e.g., in the lumped capacitors used) than what was simulated. This is consistent since all of the experimental ELC-SRR, ELC, and SRR peaks are shifted by approximately 70 MHz compared to their simulated peaks in Fig. 3. For the individual ELC and SRR results, one must remember that some of the discrepancies in performance are due to decreased coupling with the experimental TE_{10} mode wave (i.e., less flux through the SRRs compared to the plane wave simulation). In addition, the field distribution in a closed waveguide is stronger in the center than at the sides (where the SRRs are located). Thus, the experimental SRR response is weaker than the experimental ELC response in Fig. 5, in contrast to the stronger simulated SRR response in Fig. 3.

Additional design and experimentation was performed to increase the bandwidth of the ELC-SRR absorber. This was accomplished by increasing the lumped resistances on the individual ELCs and SRRs, and by sandwiching individual particles with different resonances closer together to create a denser, and more broadband absorber. One of the benefits of a low-reflection absorber design is that additional absorber can be placed in the propagation direction to increase absorption performance. However, the goal was to increase bandwidth while maintaining the same form factor as a single cell, thus sandwiching in the transverse direction was preferred. This method is more difficult because of rapidly increasing mutual inductances between the cells, especially for the magnetically coupled SRRs, which decreases ω_0 of the

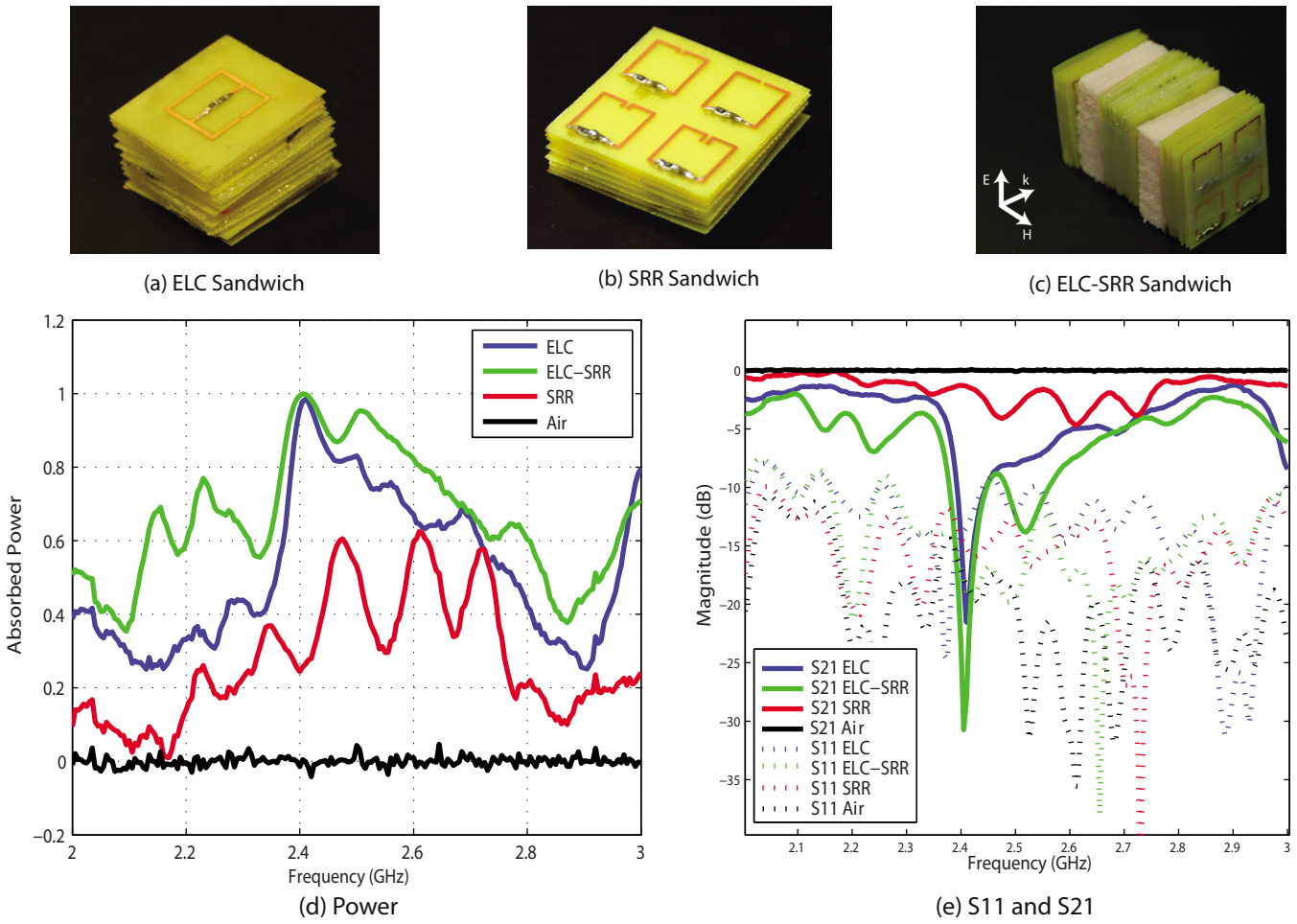

FIG. 6. (Color online) ELC-SRR sandwich experimental performance. (a) ELC sandwich. (b) SRR sandwich. (c) ELC-SRR sandwich. (d) ELC-SRR sandwich peak absorption of 99.9% at 2.4 GHz, with FWHM of 700 MHz. Distinct absorption maxima and minima are due to component particle resonances. (e) ELC-SRR sandwich absorption due to transmission (S21) decrease. S11 remains low, but varies throughout band due to imperfect matching of ELC and SRR resonances.

cells, and also blends the resonances together. Thus, multiple SRRs and ELCs with distinct individual resonances that cover a large frequency range will have a narrower frequency range when packed closely together. Another key limitation is that the absorber no longer functions if the SRRs and ELCs are mixed together in close proximity. In order to overcome these challenges, a 4-SRR cell was designed whereby only SRRs of the same resonance frequency were placed in parallel, as shown in Fig. 6(b). ELCs and SRRs were also segregated. The final structure in Fig. 6(c) was also experimentally adjusted so that the broadband ELC resonance was of similar magnitude and bandwidth as that of the SRRs.

The final ELC-SRR sandwich was able to achieve a peak absorption of 99.9% at 2.4 GHz and 700 MHz FWHM bandwidth as shown in Fig. 6(d), while maintaining low reflection of below −10 dB as shown in Fig. 6(e). The "bumpiness" in Fig. 6(d) also indicate that the ELC-SRR responses are composed of many distinct resonances, which is consistent with the fact that the ELC and SRR sandwiches were composed of 13 and 56 individual ELCs and SRRs with 13 and 10 different resonant frequencies, respectively. Note that the ELC by itself in Fig. 6(d) has a high peak absorption and bandwidth as well, although lower than the ELC-SRR at all frequencies. This unusually high absorption is likely due to the sandwiching of the ELC, since a single ELC would have substantial reflections. This is especially true at the peak of 2.4 GHz, where the close sandwiching of the ELCs may have generated enough current to create a magnetic response in the electrical-response dominated ELC such that μ_r was comparable to ϵ_r, resulting in near-perfect matching at 2.4 GHz and near perfect absorption.

IV. SUMMARY

We have thus designed, simulated, and experimentally verified the performance of a broadband low-reflection metamaterial absorber, with a peak absorption of 99.9% at 2.4 GHz, and a FWHM of 700 MHz. Although conventional rf absorbers such as pyramidal absorbers have larger bandwidths, the ELC-SRR sandwich has several advantages. One advantage of the ELC-SRR sandwich is its relatively thin ($\approx\lambda/5$) thickness in the propagation direction, compared to the typical ($\approx\lambda/2$) or greater thickness of carbon loaded foam pyramidal absorbers. The biggest advantage however, is the ability to add lumped circuit elements to introduce tunability and other active performance enhancements. For example, MEMS (Micro Electrical Mechanical Systems)

switches, varactor diodes, and other elements have been demonstrated to enable frequency tunable metamaterials.[25–28] A similar technique can be applied to the ELCs and SRRs of the ELC-SRR absorber to dynamically control its absorption properties.

[1] V. Veselago, Sov. Phys. Usp. **10**, 509 (1968).
[2] J. Pendry, A. Holden, D. Robbins, and W. Stewart, IEEE Trans. Microwave Theory Tech. **47**, 2075 (1999).
[3] D. R. Smith, W. J. Padilla, D. C. Vier, S. C. Nemat-Nasser, and S. Schultz, Phys. Rev. Lett. **84**, 4184 (2000).
[4] R. A. Shelby, D. R. Smith, and S. Schultz, Science **292**, 77 (2001).
[5] D. Schurig, J. J. Mock, and D. R. Smith, Appl. Phys. Lett. **88**, 041109 (2006).
[6] R. Liu, A. Degiron, J. J. Mock, and D. R. Smith, Appl. Phys. Lett. **90**, 263504 (2007).
[7] C. Kyriazidou, R. Diaz, and N. Alexopoulous, IEEE Trans. Antennas Propag. **48**, 107 (2000).
[8] S. Chakravarty, R. Mittra, and N. Williams, IEEE Trans. Antennas Propag. **50**, 284 (2002).
[9] N. I. Landy, S. Sajuyigbe, J. J. Mock, D. R. Smith, and W. J. Padilla, Phys. Rev. Lett. **100**, 207402 (2008).
[10] H. Tao, C. M. Bingham, A. C. Strikwerda, D. Pilon, D. Shrekenhamer, N. I. Landy, K. Fan, X. Zhang, W. J. Padilla, and R. D. Averitt, Phys. Rev. B **78**, 241103 (2008).
[11] F. Bilotti, L. Nucci, and L. Vegni, Microwave Opt. Technol. Lett. **48**, 2171 (2006).
[12] N. I. Landy, C. M. Bingham, T. Tyler, N. Jokerst, D. R. Smith, and W. J. Padilla, Phys. Rev. B **79**, 125104 (2009).
[13] J. B. Pendry, A. J. Holden, W. J. Stewart, and I. Youngs, Phys. Rev. Lett. **76**, 4773 (1996).
[14] C. R. Simovski and S. A. Tretyakov, Phys. Rev. B **75**, 195111 (2007).
[15] F. Falcone, T. Lopetegi, M. A. G. Laso, J. D. Baena, J. Bonache, M. Beruete, R. Marqués, F. Martín, and M. Sorolla, Phys. Rev. Lett. **93**, 197401 (2004).
[16] E. Shamonina, V. Kalinin, K. Ringhofer, and L. Solymar, J. Appl. Phys. **92**, 6252 (2002).
[17] H. Chen, L. Ran, J. Huangfu, T. M. Grzegorczyk, and J. A. Kong, J. Appl. Phys. **100**, 024915 (2006).
[18] D. R. Smith, D. C. Vier, N. Kroll, and S. Schultz, Appl. Phys. Lett. **77**, 2246 (2000).
[19] S. A. Cummer and B.-I. Popa, Appl. Phys. Lett. **85**, 4564 (2004).
[20] B.-I. Popa and S. A. Cummer, Phys. Rev. B **72**, 165102 (2005).
[21] D. R. Smith, D. C. Vier, T. Koschny, and C. M. Soukoulis, Phys. Rev. E **71**, 036617 (2005).
[22] R. B. Greegor, C. G. Parazzoli, J. A. Nielsen, M. A. Thompson, M. H. Tanielian, and D. R. Smith, Appl. Phys. Lett. **87**, 091114 (2005).
[23] B.-I. Popa and S. A. Cummer, Phys. Rev. E **73**, 016617 (2006).
[24] D. Schurig, J. J. Mock, B. J. Justice, S. A. Cummer, J. B. Pendry, A. F. Starr, and D. R. Smith, Science **314**, 977 (2006).
[25] O. Reynet and O. Acher, Appl. Phys. Lett. **84**, 1198 (2004).
[26] Y. He, P. He, S. D. Yoon, P. Parimi, F. Rachford, V. Harris, and C. Vittoria, J. Magn. Magn. Mater. **313**, 187 (2007).
[27] I. Gil, J. Garcia-Garcia, J. Bonache, F. Martin, M. Sorolla, and R. Marques, Electron. Lett. **40**, 1347 (2004).
[28] T. Hand and S. A. Cummer, IEEE Trans. Antennas Propag. **8**, 262 (2009).